SUPPLEMENTAL MATERIAL

Huang, J., et al., 2020, Diverse rock types detected in the lunar South Pole–Aitken Basin by the Chang'E-4 lunar mission: Geology, v. 48, https://doi.org/10.1130/G47280.1

Table S1. Model abundances of plagioclase (Pl), olivine (Ol), ortho-pyroxene (Opx) and cline-pyroxene (Cpx)

	Pl (%)	Ol (%)	Opx (%)	Cpx (%)
A	58.4 ± 0.5	8.3 ± 0.1	29.1 ± 0.4	4.2 ± 0.1
S1-1	70.7 ± 4.8	11.1 ± 2.7	9.7 ± 3.0	8.5 ± 0.8
202	54.5 ± 5.5	9.1 ± 1.1	17.3 ± 3.8	19.1 ± 0.7
207	64.3 ± 9.8	10.7 ± 2.9	17.4 ± 5.7	7.6 ± 1.1
208	75.0 ± 8.1	9.7 ± 3.7	9.7 ± 3.7	5.6 ± 0.7
301	51.7 ± 1.1	2.4 ± 2.4	27.7 ± 1.6	18.2 ± 4.4
304-1	70.2 ± 1.8	0.0 ± 0.0	18.7 ± 2.3	11.1 ± 1.0
304-2	41.5 ± 2.1	3.0 ± 3.0	30.8 ± 3.4	24.7 ± 4.1
306	75.2 ± 0.8	0.0 ± 0.0	16.7 ± 1.1	8.1 ± 1.2
308	79.3 ± 2.3	0.0 ± 0.0	4.6 ± 0.7	16.1 ± 2.3
23	55.2 ± 2.3	0.0 ± 0.0	33.7 ± 3.9	11.1 ± 1.7
24	71.0 ± 4.7	1.6 ± 1.6	0.0 ± 0.0	27.4 ± 3.7
27	83.0 ± 2.3	3.4 ± 0.5	3.9 ± 1.4	9.7 ± 0.5
28	68.2 ± 4.1	5.6 ± 1.6	12.7 ± 1.6	13.5 ± 2.2
29	47.4 ± 2.1	5.3 ± 0.2	31.5 ± 1.2	15.8 ± 0.6
31	72.7 ± 1.1	2.1 ± 1.2	16.4 ± 0.7	8.8 ± 0.9
32	62.4 ± 1.5	2.0 ± 2.0	18.8 ± 0.8	16.8 ± 1.2

Table S2. Locations and source images for orbital Moon Mineralogy Mapper (M3) spectra shown in Fig. S1D.

Location	Latitude, Longitude	M3 Observations
Fresh Mare	176.41121°E, -45.42548°N	M3G20090720T003411 M3G20090816T045833
Landing Site	177.54958°E, -45.41561°N 177.55317°E, -45.49568°N 177.58851°E, -45.45653°N 177.61997°E, -45.41469°N 177.62288°E, -45.49568°N	M3G20090622T124051 M3G20090719T200620 M3G20090720T003411 M3G20090816T045833
Finsen Ejecta	179.82839°E, -43.09459°N	M3G20081129T052459 M3G20090622T082242 M3G20090622T124051 M3G20090719T160300 M3G20090719T200620 M3G20090816T005433 M3G20090816T045833
Finsen Ejecta	-179.72070°E, -42.94123°N	M3G20081129T052459 M3G20090622T082242 M3G20090719T160300 M3G20090719T200620 M3G20090816T005433
Finsen Rim	-178.87078°E, -42.60877°N	M3G20081129T052459 M3G20090719T160300 M3G20090815T202602 M3G20090816T005433
Finsen Peak	-177.49733°E, -42.43186°N	M3G20090622T041041 M3G20090622T082242 M3G20090719T113510 M3G20090719T160300 M3G20090815T202602

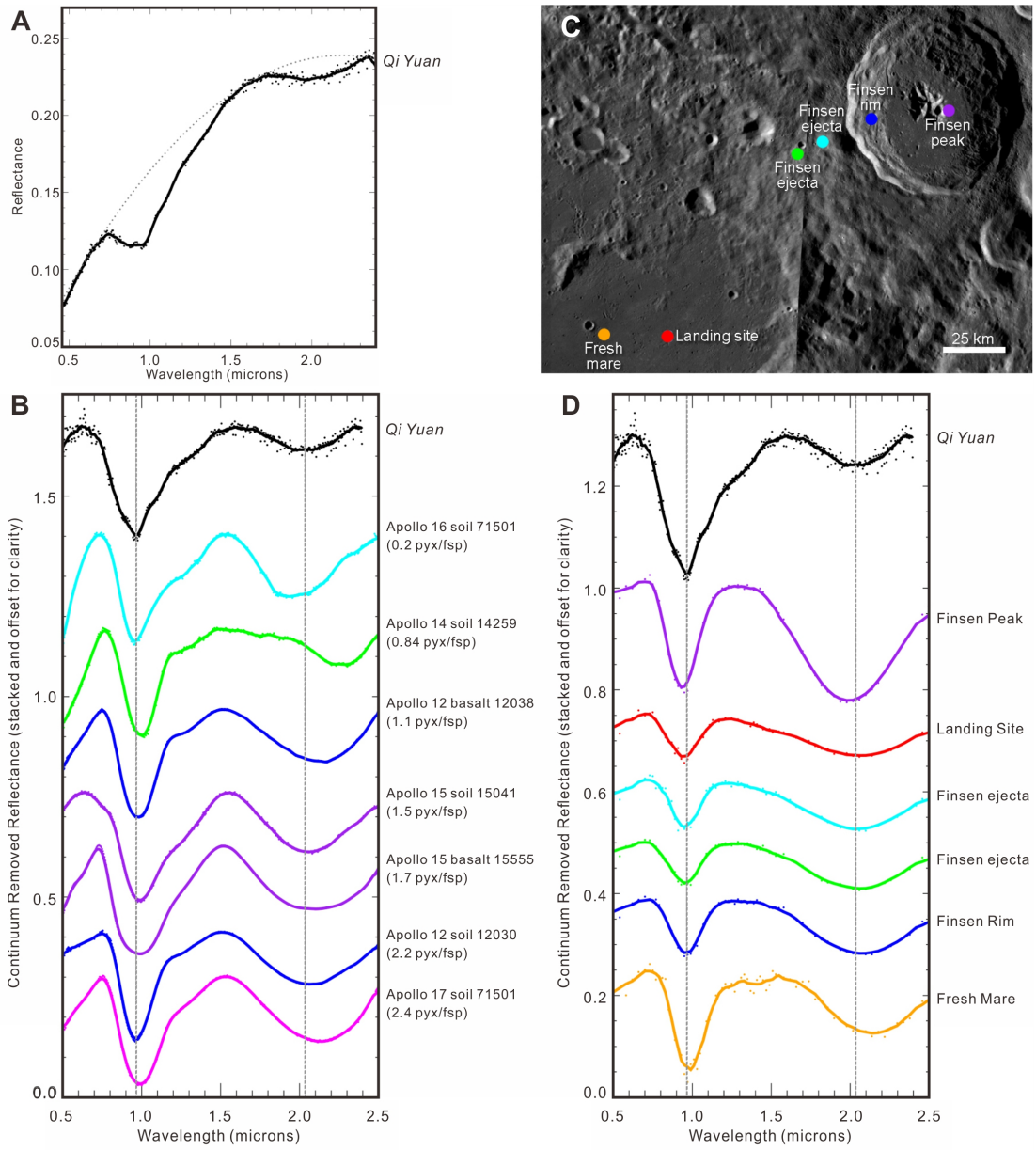

Figure S1. VNIS spectrum of *Qi Yuan* compared to Apollo samples and M3 spectra. (A) Reflectance spectrum of *Qi Yuan*, showing parabolic continuum fit (dashed line). (B) Comparison of continuum removed spectra of *Qi Yuan* and spectrally similar Apollo samples. Dashed vertical lines indicate band centers for *Qi Yuan*. (C) Regional NAC mosaic showing locations where M3 spectra were extracted. (D) Comparison of continuum removed spectra of *Qi Yuan* and M3 spectra from locations shown in (C). *Qi Yuan* is most similar to M3 spectra from the crater rim and proximal ejecta.

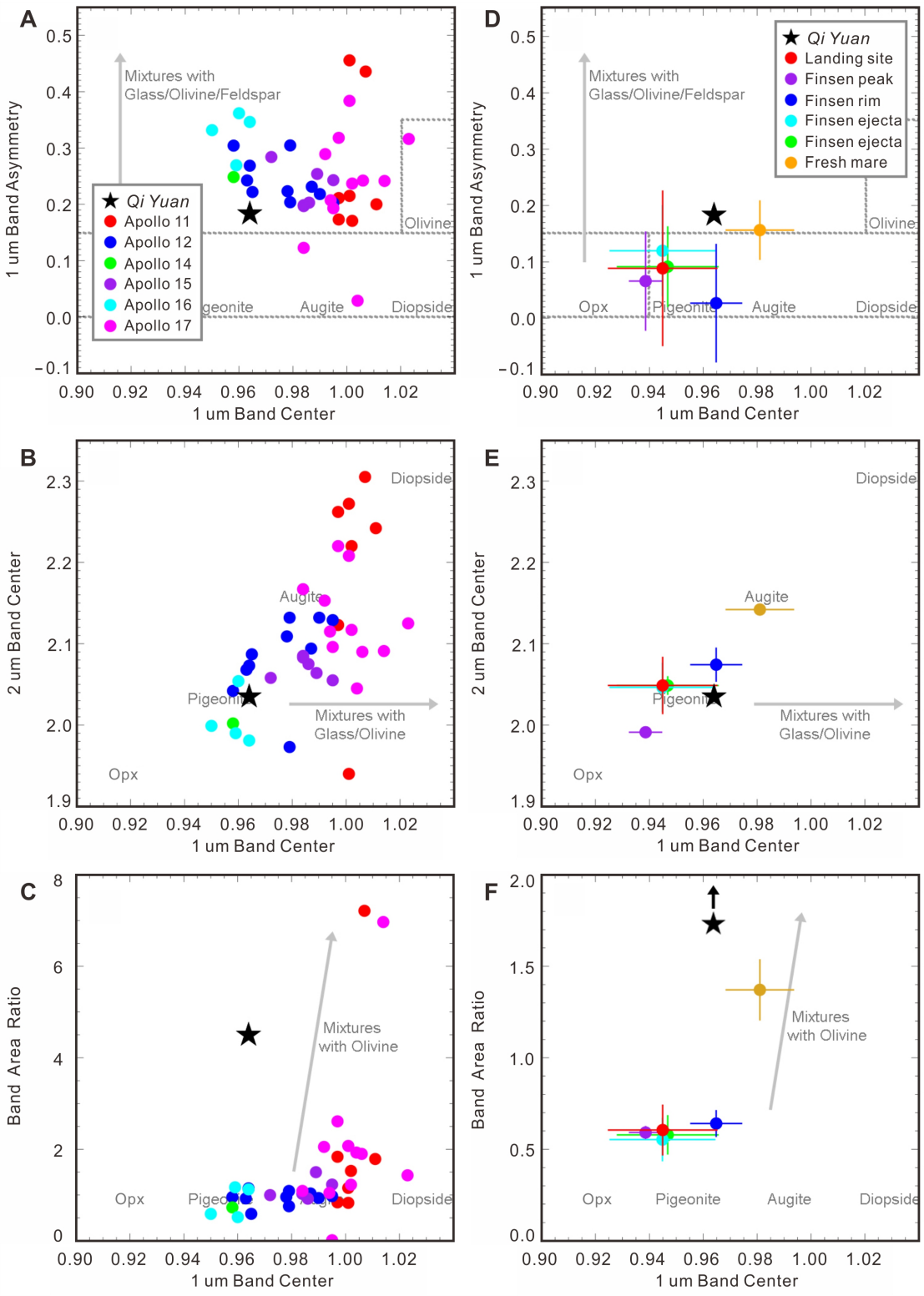

Figure S2. Comparison of 1 and 2 micron band parameters as calculated for *Qi Yuan* (start), (A-C) Apollo samples, and (D-F) M3 spectra, where points indicate mean of all spectra from all cubes at that location, and error bars indicate one standard deviation in parameters. (A) Apollo samples

exhibit a relatively narrow range of 1 micron band parameters, consistent with variations on the assemblage orthopyroxene/clinopyroxene/olivine/plagioclase, but samples most similar to *Qi Yuan* are typically dominated by pigeonite and plagioclase. (B) The linear trend in the 1 and 2 micron band centers of Apollo samples is consistent with variations in pyroxene composition, with *Qi Yuan* falling within the range consistent with pigeonite. (C) High ratios of the 1 and 2 micron band areas are a good indicator of olivine, although *Qi Yuan*'s large area ratio relative to otherwise similar Apollo samples may be due to low spectral contrast. (D-E) *Qi Yuan* exhibits band parameters most similar to the rim of Finsen crater, consistent with a mixture of Opx/Cpx or pigeonite. (F) The band area ratio of all M3 spectra in the Finsen peak, rim, and ejecta is low, indicating low contribution from olivine, while the fresh mare may include some contribution from olivine.

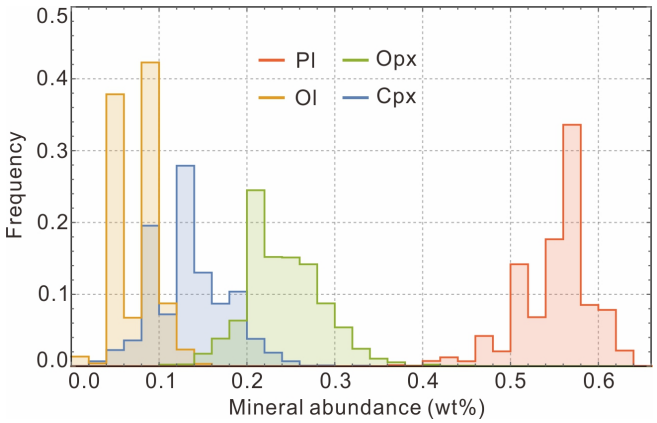

Figure S3. Pl, Ol, Opx and Cpx abundances frequency (Lemelin et al., 2016) in an area of 0.1° by 0.1° centered by the CE-4 landing point.

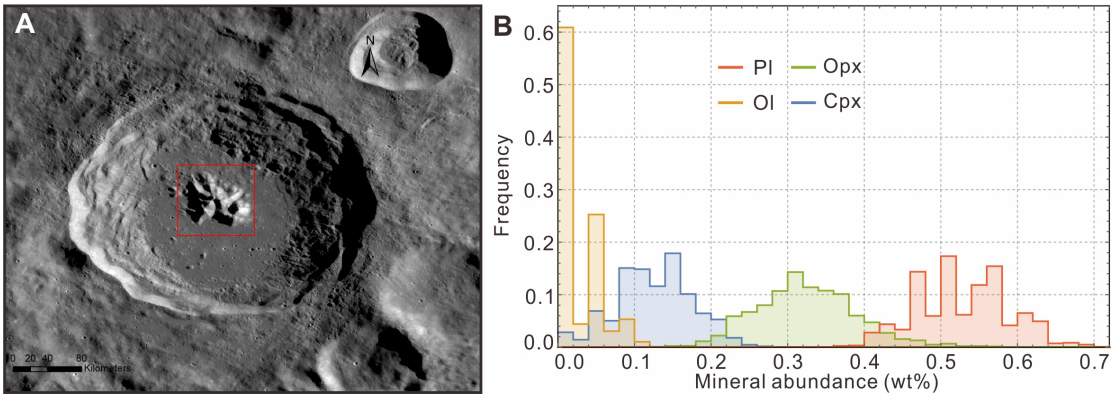

Figure S4. Mineral abundances of the Finsen central peak region. (A) Area for mineral abundances statistics of the Finsen central peak region. (B) Pl, Ol, Opx and Cpx abundances statistics (Lemelin et al., 2016) of the Finsen central peak region.

METHODS

Instrument

The VNIS instrument onboard CE-4 is a backup of the one equipped on CE-3. It consists of a 100-band Complementary Metal-Oxide Semiconductor (CMOS) imager with 256 by 256 pixels at a wavelength range of 0.45-0.95 μm and 300-band short-wavelength near-infrared (SWIR) single pixel detector at a wavelength range of 0.90-2.40 μm (Li et al., 2019). The physical detection area of the SWIR detector is a circle with the center of (96, 128) and a diameter of 107 pixels on the CMOS field of view (Fig. 3c). The VNIS instrument is mounted at a height of 0.69 meter on Yutu-2 and making observations of the surface at an angle of 45º. The dimension of the CMOS image is roughly 15 by 21 cm. All the spectra data have been processed and calibrated following a standard procedure.

VNIS data processing

We process the VNIS data from level 0B and level 1. We carry out dark current, flat-field, temperature corrections and radiometric calibration (Wu and Hapke, 2018; Li et al., 2019). Then we connected averaged spectra obtained from CMOS detector and the spectrum obtained from SWIR detector for each measurement point, using the SWIR spectra at 900 nm to correct the step artifacts due to different response in CMOS and SWIR detectors. Then we calibrate the spectra to relative reflectance using solar irradiance (Gueymard, 2004) following the procedures (Zhang et al., 2015).

For the regolith, we remove the continuum by subtracting the connecting line of reflectance values between 750 to 1550 nm. We generate a lunar spectral mineral lookup table (LUT) from 750 to 1550 nm using a radiative transfer model (Denevi et al., 2008; Lucey, 2004; Lucey et al., 2014). The grain size was fixed to be 17 μm (Pieters et al., 1993) and Mg number was fixed to be 65 (Lucey et al., 2014). We use minimum absolute difference (ABS, eq. 1), normalized absolute difference (NABS, eq. 2), centered pattern root mean square (CPRMS, eq. 3) (Taylor, 2001) and the spectral angle mapper (SAM, eq. 4) to evaluated the spectral fitting:

$$ABS = \sum_{n=1}^{N} \left| f_n - r_n \right| \tag{1}$$

$$NABS = \sum_{n=1}^{N} \left| \frac{f_n}{\bar{f}} - \frac{r_n}{\bar{r}} \right| \tag{2}$$

$$CPRMS = \sqrt{\frac{1}{N} \sum_{n=1}^{N} [(f_n - \bar{f}) - (r_n - \bar{r})]^2} \tag{3}$$

$$SAM = \frac{\sum_{i=1}^{N} f_n r_n}{\sqrt{\sum_{i=1}^{N} f_n^2} \sqrt{\sum_{i=1}^{N} r_n^2}} \quad (4)$$

where f_n, r_n, $\bar{f}$ and $\bar{r}$ are the nth measurement data, nth model prediction, average of measurement and average of model prediction of N discrete data points, respectively. We adopt the average values of the four methods as the best fit value for mineral abundance, and the errors are calculated as the standard deviation of fit values of the four methods. The LUT method does not derive the abundances of opaque minerals or glassy components, so all the mineral abundances are normalized to 100%.

Band parameter analysis

Apollo sample spectra shown in Fig. S1 were acquired from the NASA Planetary Data System (PDS) geosciences spectral library (Moriarty and Pieters, 2016). Orbital spectra are from the Moon Mineralogy Mapper (Pieters et al., 2009), an orbital imaging visible/near-infrared (0.42-3.0 μm) spectrometer and were acquired as Level 2 (reflectance) spectra from the PDS. Locations of points shown in Fig. S1 are listed in Table S2. All spectra shown are averages of all spectra at that location from all optical periods, as determined using the LROC Quickmap tool (https://quickmap.lroc.asu.edu), varying from 2 to 6 separate observations. The landing site location displayed significant variability across observations, and so was further averaged with 4 other locations surrounding the landing site at ~1.5 km radial distance.

Band parameters for *Qi Yuan*, Apollo samples, and M3 spectra were derived from continuum removed spectra, where the continuum was fitted as a second order polynomial convex hull to tie points adjusted to maximize band area near 0.7, 1.5 and 2.5 microns (2.35 microns for the VNIS spectrum), similar to the process described for a linear convex hull in Bennett et al. (2016). Band parameters (center, asymmetry, and area) were calculated using the methods of Horgan et al. (2014). Mineral interpretations were based on comparison to parameters for laboratory spectra analyzed by Cloutis & Gaffey (1991), Klima et al., (2007), Klima et al., (2011), Horgan et al. (2014), and Viviano et al. (2019).

Comments on the CE-4 olivine-rich material observations by Li et al., (2019)

A recent study reported mantle-derived materials identified by the CE-4 VNIS observations on Li et al., (2019). The mineral abundances for low-Ca pyroxene (LCP)/high-Ca Pyroxene (HCP)/Olivine are reported to be 42%/10%/48%, and 38%/7%/55% for spectra CE4_0015 and CE4_0016, respectively. However, the elevated olivine abundances of Li et al., (2019) are inconsistent with the Kaguya MI mineral abundance maps over the landing region (Fig. S3), and

with our results: 59% Pl, 8% Ol, 29% Opx, 4% Cpx for CE4_0015 and 71% Pl, 11% Ol, 10% Opx, 8% Cpx for CE4_0016. Even the central peak of the Finsen crater does not have close abundance of olivine (Fig. S4) comparing to the results of Li et al., (2019). Li et al., (2019) used four mineral assemblages (LCP+HCP+Ol, LCP+HCP+Pl, LCP+Pl, LCP+Ol), however, a common mineral assemblage of LCP+HCP+Ol+Pl was not included in the MGM deconvolution. Pl and Ol have very similar spectral features around 1250 nm, which makes MGM deconvolution difficult to resolve the abundance of Pl. In addition, the RMS Error of mineral assemblage LCP+HCP+Pl is only 20% larger than that of LCP+HCP+Ol, which is comparable to the uncertainty of the MGM deconvolution method. In addition, Li et al., (2019) mentioned "The overall spectral shape and absorption-band positions are more similar to those of lunar highland materials", which also contradicts with the reported mineral abundances in their study.

Data Availability

All the data are provided in Source Data. Datasets generated or analyzed during this study are available from the corresponding author upon reasonable request.

REFERENCES CITED

Bennett, K. A., Horgan, B. H., Gaddis, L. R., Greenhagen, B. T., Allen, C. C., Hayne, P. O., Bell III, J. F., and Paige, D. A., 2016, Complex explosive volcanic activity on the Moon within Oppenheimer crater: Icarus, v. 273, p. 296-314.

Cloutis, E. A., and Gaffey, M. J., 1991, Pyroxene spectroscopy revisited: Spectral-compositional correlations and relationship to geothermometry: Journal of Geophysical Research: Planets, v. 96, no. E5, p. 22809-22826.

Denevi, B., Lucey, P., and Sherman, S., 2008, Radiative transfer modeling of near-infrared spectra of lunar mare soils: Theory and measurement: Journal of Geophysical Research: Planets, v. 113, no. E2.

Gueymard, C. A., 2004, The sun's total and spectral irradiance for solar energy applications and solar radiation models: Solar energy, v. 76, no. 4, p. 423-453.

Horgan, B. H., Cloutis, E. A., Mann, P., and Bell III, J. F., 2014, Near-infrared spectra of ferrous mineral mixtures and methods for their identification in planetary surface spectra: Icarus, v. 234, p. 132-154.

Klima, R. L., Pieters, C. M., & Dyar, M. D., 2007. Spectroscopy of synthetic Mg-Fe pyroxenes I: Spin-allowed and spin-forbidden crystal field bands in t he visible and near-infrared. Meteoritics & Planetary Science, 42(2), 235-253.

Klima, R. L., Dyar, M. D., & Pieters, C. M., 2011. Near-infrared spectra of clinopyroxenes: Effects of calcium content and crystal structure. Meteoritics & Planetary Science, 46(3),

379-395.

Lemelin, M., Lucey, P., Gaddis, L., Hare, T., and Ohtake, M., Global map products from the Kaguya multiband imager at 512 ppd: Minerals, FeO, and OMAT, *in* Proceedings Lunar and Planetary Science Conference2016, Volume 47, p. 2994.

Li, C., Liu, D., Liu, B., Ren, X., Liu, J., He, Z., Zuo, W., Zeng, X., Xu, R., and Tan, X., 2019, Chang'E-4 initial spectroscopic identification of lunar far-side mantle-derived materials: Nature, v. 569, no. 7756, p. 378.

Li, C. L., Xu, R., Lv, G., Yuan, L. Y., He, Z. P., & Wang, J. Y. (2019). Detection and calibration characteristics of the visible and near-infrared imaging spectrometer in the Chang'e-4. Review of Scientific Instruments, 90(10), 103106.

Ling, Z., Jolliff, B. L., Wang, A., Li, C., Liu, J., Zhang, J., Li, B., Sun, L., Chen, J., and Xiao, L., 2015, Correlated compositional and mineralogical investigations at the Chang′ e-3 landing site: Nature communications, v. 6, p. 8880.

Lucey, P. G., 2004, Mineral maps of the Moon: Geophysical Research Letters, v. 31, no. 8.

Lucey, P. G., Norman, J. A., Crites, S. T., Taylor, G. J., Hawke, B. R., Lemelin, M., and Melosh, H. J., 2014, A large spectral survey of small lunar craters: Implications for the composition of the lunar mantle: American Mineralogist, v. 99, no. 11-12, p. 2251-2257.

Moriarty III, D., and Pieters, C., 2016, Complexities in pyroxene compositions derived from absorption band centers: Examples from Apollo samples, HED meteorites, synthetic pure pyroxenes, and remote sensing data: Meteoritics & Planetary Science, v. 51, no. 2, p. 207-234.

Pieters, C. M., Boardman, J., Buratti, B., Chatterjee, A., Clark, R., Glavich, T., Green, R., Head III, J., Isaacson, P., and Malaret, E., 2009, The Moon Mineralogy Mapper (M^3) on Chandrayaan-1: Current Science, p. 500-505.

Pieters, C. M., Fischer, E. M., Rode, O., and Basu, A., 1993, Optical effects of space weathering: The role of the finest fraction: Journal of Geophysical Research: Planets, v. 98, no. E11, p. 20817-20824.

Taylor, K. E., 2001, Summarizing multiple aspects of model performance in a single diagram: Journal of Geophysical Research: Atmospheres, v. 106, no. D7, p. 7183-7192.

Viviano, C. E., Murchie, S. L., Daubar, I. J., Morgan, M. F., Seelos, F. P., and Plescia, J. B., 2019, Composition of Amazonian volcanic materials in Tharsis and Elysium, Mars, from MRO/CRISM reflectance spectra: Icarus, v. 328, p. 274-286.

Wu, Y., & Hapke, B. 2018. Spectroscopic observations of the Moon at the lunar surface. Earth and Planetary Science Letters, 484, 145-153.

Zhang, H., Yang, Y., Yuan, Y., Jin, W., Lucey, P. G., Zhu, M. H., Kaydash, V. G., Shkuratov, Y. G., Di, K., and Wan, W., 2015, In situ optical measurements of Chang'E-3 landing site in

Mare Imbrium: 1. Mineral abundances inferred from spectral reflectance: Geophysical Research Letters, v. 42, no. 17, p. 6945-6950.